

Resolving Galactic Rotation Curve Discrepancies Through a Proposed Observation Effect

Brahim Benaissa
ORCID:0000-0002-9472-9331

March 18, 2025

Abstract

If an observational effect induces an apparent spatial compression of galaxies, it may account for the discrepancies in their observed orbital speeds. This study investigates whether the flat rotation curve arise from such an observational effect rather than requiring dark matter or modifications to gravity. Using an inverse problem approach, we demonstrate that Newtonian dynamics remain consistent with observed rotation curves when incorporating a radially dependent space scale factor that maps true spatial dimensions to observed ones. Analyzing 175 galaxies from the SPARC dataset, we find that the intrinsic curvature associated with this apparent compression exhibits a strong correlation with the Ricci curvature derived from the baryonic mass distribution. All results and code associated with this study are available for review and further analysis.

Keywords: Galactic Rotation Curves, Dark Matter, Observation Effect, Space-time Curvature.

1 Introduction

This paper addresses the discrepancy between the observed orbital velocities of stars in galaxies and those predicted by Newtonian mechanics. The flat rotation curves observed at large galactic radii imply the existence of missing mass, typically attributed to dark matter or solved by modifications to gravitational theory [1, 2, 3]. While the dark matter hypothesis remains incomplete, with multiple proposed particle candidates, it continues to serve as the primary framework for explaining the anomalies in galactic rotation curves [4].

Given that direct detection of dark matter particles has not yet been achieved, despite extensive experimental efforts [5], it has become necessary to explore alternative theoretical frameworks. This study investigates the possibility that

an observational effect causes galaxies to appear spatially compressed, influencing how their rotation curves are measured. This implies that the actual spatial extent of the galaxy is larger than our perception suggests.

This effect has a significant impact: the rotational velocities of stars in distant galaxies may be underestimated because the stars travel greater distances than our measurements indicate. Similarly, the observed orbital radius of a star appears smaller than its actual radius, leading to lower inferred velocities. Additionally, this effect reduces the apparent angular sizes and inferred distances, causing their luminosities to be underestimated and, consequently, leading to an underestimation of their true masses.

The SPARC dataset (Spitzer Photometry and Accurate Rotation Curves) provides rotation curves for 175 nearby galaxies, compiled from several relatively homogeneous studies. These curves were analyzed for large-scale features that correlate with the galaxies' surface brightness profiles. The analysis included procedures to remove contaminants like foreground stars and background galaxies, as well as to minimize errors, such as those caused by beam-smearing effects [?].

An inverse problem approach is employed to reconcile rotation curves using an iterative search algorithm. This method minimizes the discrepancy between Newtonian predictions, which consider only baryonic mass, and the observed velocities. This apparent compression effect is calculated by scaling the Newtonian rotation curves by two parameters: a constant mass coefficient and a radially dependent scale factor. This approach will allow us to test the validity of the suggested effect as an explanation for the observed discrepancies in rotational velocities.

2 Inverse problem Approach

The distortion in perceived spatial scale is quantified by the *space scale factor* $\xi(r)$, which relates the true length $l_{\text{true}}(r)$ at radius r to its observed length $l_{\text{obs}}(r)$ at the same radius:

$$l_{\text{true}}(r) = \xi(r) \cdot l_{\text{obs}}(r) \tag{1}$$

The space scale factor ξ , when equal to 1 relative to the observer's scale, indicates that the observed velocity is identical to the true velocity of an object. This means there is no distortion or scaling effect altering the measurement. According to the hypothesis proposed in this study, the value of ξ is expected to increase and reach its maximum at the galactic center. This suggests that spatial scaling effects become most pronounced in this region, potentially influencing velocity measurements. The true velocity of a star $v_{\text{true}}(r)$ should correspond to the scaled observed velocity $v_{\text{obs}}(r)$:

$$v_{\text{obs}}(r) = \frac{v_{\text{true}}(r)}{\xi(r)} \tag{2}$$

To interpret observed rotation curves through the suggested observation effect. This work assumes that baryonic matter constitutes the total mass, and the galactic rotation adheres to Newtonian dynamics, thus here $v_{\text{true}} = v_{\text{Newt}}$.

The discrepancies between observed velocities and Newtonian predictions are reconciled via the space scale factor. The analysis calculates this factor through iterative optimization process, that minimize of the deviations between scaled Newtonian velocities and observed velocities. The Newtonian velocity $v_{\text{Newt}}(r)$ is calculated based on baryonic mass:

$$v_{\text{Newt}}(r) = \sqrt{\frac{GM_{\text{bary}}(r)}{r}} \quad (3)$$

The total baryonic mass of each galaxy is derived from its luminous components, disk and bulge, assuming exponential and Hernquist profiles respectively [?, ?]. These profiles are used to compute the enclosed mass at observed radii. The disk mass is modeled using an exponential surface density profile. The enclosed mass at radius r is given by [?]:

$$M_{\text{disk}}(r) = M_{\text{disk}}^{\text{total}} \left[1 - \left(1 + \frac{r}{R_{\text{disk}}} \right) e^{-r/R_{\text{disk}}} \right] \quad (4)$$

$$M_{\text{bulge}}(r) = M_{\text{bulge}}^{\text{total}} \left(\frac{r}{r+a} \right)^2, \quad \text{with} \quad a = \frac{R_{\text{eff}}}{1.8153} \quad (5)$$

$$M_{\text{bary}}(r) = M_{\text{disk}}(r) + M_{\text{bulge}}(r) \quad (6)$$

The suggested observation effect introduces two principal modifications to reconcile observed galactic rotation velocities with Newtonian predictions. First, a uniform mass coefficient μ is applied to the enclosed baryonic mass to correct the systematic underestimation of the luminous mass. This adjustment is consistent with the assumption of an underlying exponential mass distribution. Second, a radial scaling factor $\xi(r)$ adjusts the observed velocities at different radii.

These parameters are simultaneously optimized by the YUKI algorithm, which iteratively minimizes the Euclidean norm of the discrepancy between the scaled Newtonian velocities $v_{\text{fit}}(r)$ and the observed velocities $v_{\text{obs}}(r)$, where n is the number of radii for each galaxy. Consequently, the values of μ and $\xi(r)$, corresponding to the fitted velocity, are computed.

$$V_{\text{fit}}(r) = \sqrt{\frac{G(\mu \cdot M_{\text{bary}}(r))}{r}} \cdot \frac{1}{\xi(r)} \quad (7)$$

$$\text{Objective function} = \sqrt{\sum_{i=1}^n \left(V_{\text{fit}}^i(r) - v_{\text{obs}}^i(r) \right)^2} \quad (8)$$

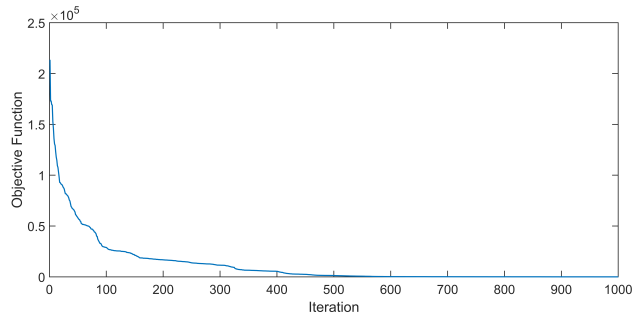


Figure 1: Convergence of the objective function across iterations for galaxy NGC7793.

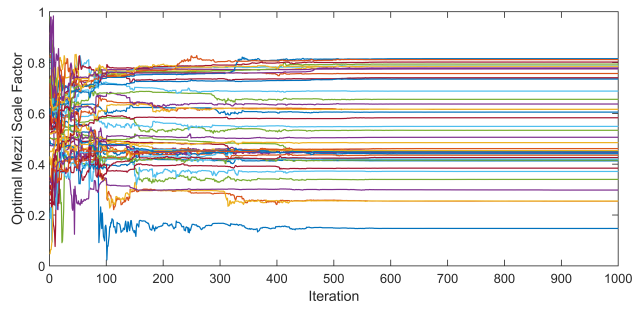


Figure 2: Convergence of the space scale factor $\xi(r)$ across iterations.

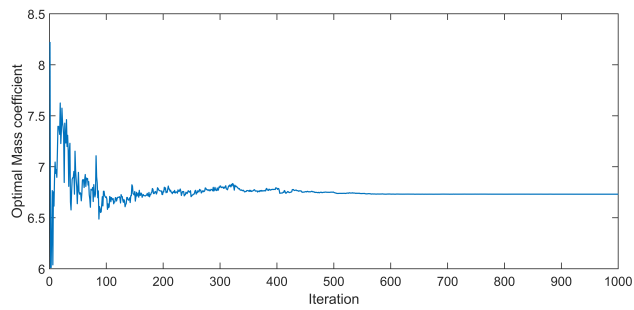


Figure 3: Convergence of the mass coefficient μ across iterations.

The YUKI algorithm employs a dynamic search space reduction strategy by defining a local search region around the best identified solutions. Exploitation focuses on refining promising solutions by gradually adjusting candidates within the local search region. Meanwhile, exploration introduces diversity by searching outside the local search region, which helps avoid converging to local optima. By these two strategies, this algorithm effectively tackles large scale global problems across various domains [?]

The space scale factor ξ , is defined such that it is equal to 1 in regions where the space scale distortion is negligible, and has no upper limit. This allow the exploration of all possible values to determine the extent to which the distortion can affect observations, thus we considered $1/\xi(r)$ constrained between 0 and 1. The minimum mass coefficient μ is set 1 and the maximum value is set to an exaggerated value of 100.

The algorithm parameters are systematically defined as follows: the number of iterations is set to 50000, the search population is 20, and EXP, the parameter that determines the percentage of solutions allocated for exploration, is set to 0.99.

Figure 1 illustrates the convergence of the objective function for the galaxy NGC7793, highlighting the reduction of the error between the scaled Newtonian rotation curve and the observed rotation curve as the algorithm progresses. Figure 2 shows the convergence of the space scale factor in each radius $\xi(r)$. Figure 3 presents the convergence of the mass coefficient μ .

3 Space Scale Factor and Curvature

The intrinsic curvature of the suggested effect can be expressed by the Gaussian curvature $K(r)$ [?]. With $\xi(r)$ is the predicted space scale factor at the observed radius r .

$$K(r) = \frac{\xi(r)}{r^2} \quad (9)$$

On the other hand, the Ricci scalar curvature $R(r)$ is calculated from the enclosed mass gradient [?]:

$$R(r) = \frac{2G}{c^2 r^2} \frac{\partial M_{\text{bary}}(r)}{\partial r} \quad (10)$$

The findings are classified into three categories based on the space scale factor:

1. **Expected Behavior:** In 135 galaxies, the space scale factor exhibits the anticipated trend, peaking near the galactic center and decreasing toward the outer edges. An example of this behavior is shown in Figure 4
2. **Deviations from the Expected Trend:** In 37 galaxies, the expected trend is still observed, but with deviations beginning near the galactic center

and extending to various radii. Among these, 16 galaxies show minor deviations, while 20 galaxies display significant deviations. Figure 5 illustrates an example of a minor deviation, while Figure 6 shows an example of a major deviation.

3. **Reversed Behavior:** In 3 galaxies, the space scale factor increases from the galactic center toward the outer edge, which contrasts with the expected trend. An example of this reversed behavior is shown in Figure 7.

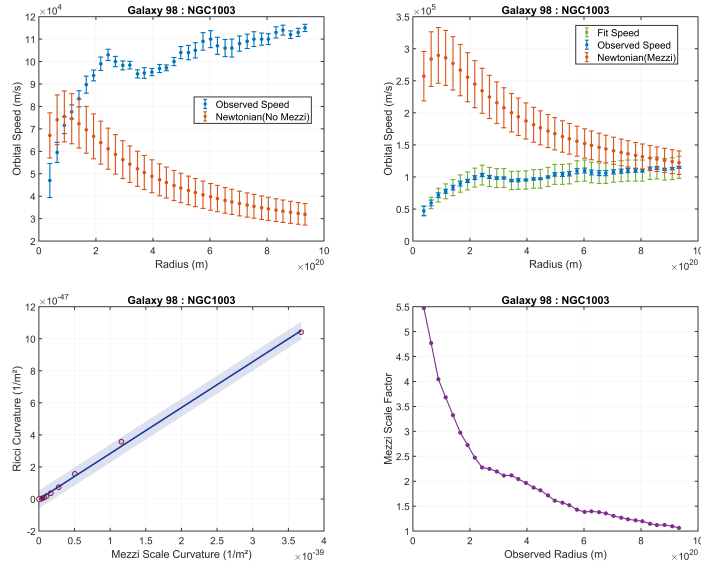


Figure 4: Comparison of observed and theoretical rotation curves with and without the suggested effect in Galaxy NGC1003 (Expected).

In galaxies displaying a reversed scaling trend, the discrepancies are similar to those found in large deviation cases, but with a much larger divergence between the observed velocities and the Newtonian velocities (excluding the suggested effect). This indicates a more pronounced departure from conventional Newtonian predictions. Within the context of this study, these deviations indicate that observed velocities may be significantly affected by accumulated distance underestimation errors, which could introduce substantial distortions in the inferred orbital dynamics, this is backed by the following observation.

Each of Figures 4–7 comprises four subfigures:

- Top-left: Compare the observed rotation curve with the Newtonian prediction that does not account for the suggested effect, showing discrepancies between Newtonian and observed rotation curves.

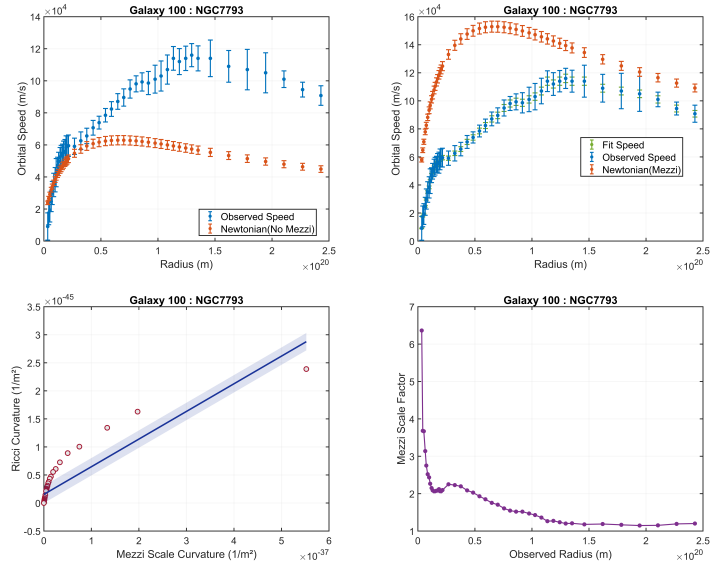


Figure 5: Comparison of observed and theoretical rotation curves with and without the suggested effect in Galaxy NGC7793 (Minor Deviation).

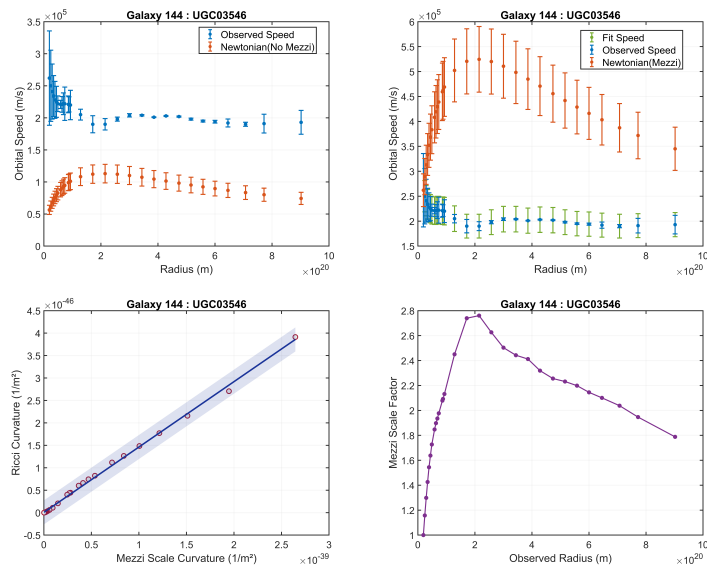


Figure 6: Comparison of observed and theoretical rotation curves with and without the suggested effect in Galaxy UGC03546 (Major Deviation).

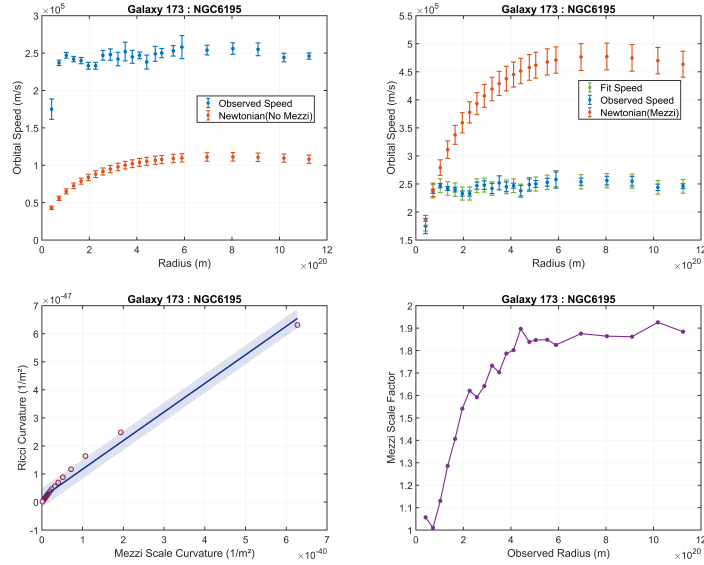


Figure 7: Comparison of observed and theoretical rotation curves with and without the suggested effect in Galaxy NGC6195 (Reversed).

- Top-right: Displays the observed rotation curve alongside the Newtonian rotation curves that incorporate the suggested effect. This comparison illustrates the true velocities based on our assumptions in relation to the observed velocities.
- Bottom-left: Displays a curvature relationship graph, showing the intrinsic curvature of the suggested effect on the x-axis and the Ricci curvature on the y-axis. A linear fit is overlaid, with a confidence region indicating a correlation level of 0.98.
- Bottom-right: Depicts the space scale factor at various radii, highlighting its spatial variation across the galaxy.

Although there exist galaxies that do not perfectly conform to the expected space scale factor trend, all galaxies exhibit a high correlation between the intrinsic curvature of the suggested effect and Ricci curvature calculated from the observed masses and radii. The lowest correlation is observed in galaxy NGC7793, shown in Figure 5, where the correlation falls below 0.9 (See figure 8). The suggested effect curvature $K(r)$ and the Ricci curvature $R(r)$ are associated in the way they reflect the observation.

These high correlations imply that the same geometric behavior responsible for the Ricci scalar results is also dictating the observational underestimation in spatial scale.

Figure 9 illustrates the mass coefficients for each galaxy, ranging from 2.5 for the galaxy UGC06667 to 79.17 for galaxy NGC2915. The average mass

coefficient is 11.35, which implies that the overall unaccounted baryonic mass could be an order of magnitude greater than what our observations currently suggest.

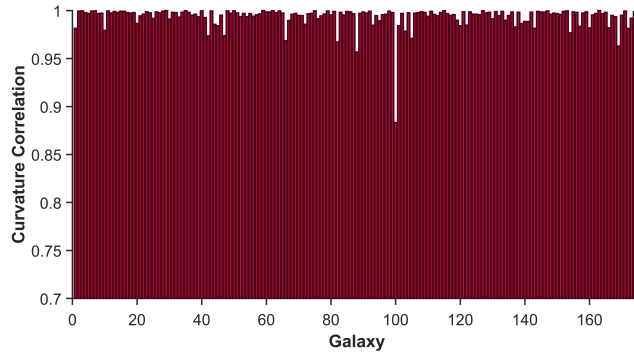


Figure 8: Correlation between the suggested effect curvature $K(r)$ and Ricci curvature $R(r)$.

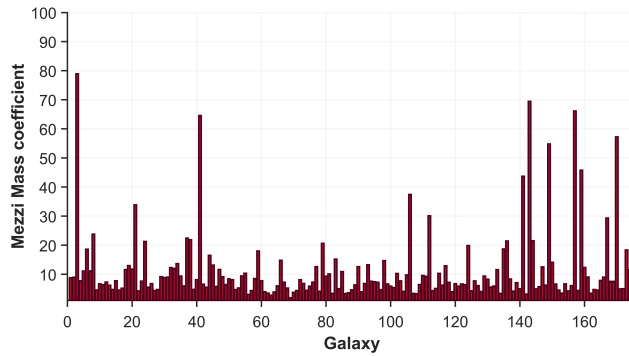


Figure 9: Predicted mass coefficient μ for each galaxy.

4 Discussion

This study presents an observation effect as a novel framework to address the discrepancies in galactic rotation curves without relying on dark matter or modifications to gravitational laws. The analysis of SPARC galaxies demonstrates that the suggested effect reconciles observed rotation curves with Newtonian predictions.

Based on this dataset, the results of this work suggest that the amount of unaccounted mass is possibly twice that predicted by current dark matter models.

While implying that the baryonic mass constitutes the entirety of the mass, and that no additional dark matter exists.

A key outcome of our study is the observed high correlation between the curvature emerging from the apparent compression effect and the Ricci curvature derived from the baryonic matter distribution. This indicates that the geometric behavior responsible for Ricci curvature is also manifest in the suggested apparent spatial compression.

References

- [1] M. Khelashvili, A. Rudakovskiy and S. Hossenfelder, Dark matter profiles of SPARC galaxies: a challenge to fuzzy dark matter, *Monthly Notices of the Royal Astronomical Society* 523, no. 3 (2023): 3393-3405.
- [2] L. Wang and D.-M. Chen, Comparison of Modeling SPARC spiral galaxies' rotation curves: halo models vs. MOND, *Research in Astronomy and Astrophysics* 21, no. 11 (2021): 271.
- [3] P. Li, F. Lelli, S. McGaugh and J. Schombert, A comprehensive catalog of dark matter halo models for SPARC galaxies, *The Astrophysical Journal Supplement Series* 247, no. 1 (2020): 31.
- [4] J. L. Feng, Dark matter candidates from particle physics and methods of detection, *Annual Review of Astronomy and Astrophysics* 48, no. 1 (2010): 495-545.
- [5] M. Misiaszek and N. Rossi, Direct detection of dark matter: A critical review, *Symmetry* 16, no. 2 (2024): 201.
- [6] F. Lelli, S. S. McGaugh and J. M. Schombert, SPARC: Mass models for 175 disk galaxies with Spitzer photometry and accurate rotation curves, *The Astronomical Journal* 152, no. 6 (2016): 157.
- [7] K. C. Freeman, On the disks of spiral and S0 galaxies, *Astrophysical Journal* 160 (1970): 811.
- [8] L. Hernquist, An analytical model for spherical galaxies and bulges, *Astrophysical Journal*, Part 1 (ISSN 0004-637X), vol. 356, June 20, 1990, p. 359-364. 356 (1990): 359-364.
- [9] J. Binney and S. Tremaine, *Galactic Dynamics*, Princeton University Press, 2011.
- [10] B. Benaissa, M. Kobayashi, M. Al Ali, S. Khatir and M. Shimoda, A novel exploration strategy for the YUKI algorithm for topology optimization with metaheuristic structural binary distribution, *Engineering Optimization* (2024): 1-21.

- [11] C. D. Modes, K. Bhattacharya and M. Warner, Gaussian curvature from flat elastica sheets, *Proceedings of the Royal Society A: Mathematical, Physical and Engineering Sciences* 467, no. 2128 (2011): 1121-1140.
- [12] H. Stephani, D. Kramer, M. MacCallum, C. Hoenselaers and E. Herlt, *Exact Solutions of Einstein's Field Equations*, Cambridge University Press, 2009.